Degradation of self-assembled monolayers in organic photovoltaic devices

CrossMark

Felipe A. Angel [a,1], Yekaterina L. Lyubarskaya [a,1], Alexander A. Shestopalov [b,*], Ching W. Tang [a,b,*]

[a] University of Rochester, Department of Chemistry, Rochester, NY 14627, USA
[b] University of Rochester, Department of Chemical Engineering, Rochester, NY 14627, USA

ARTICLE INFO

ABSTRACT

Self-assembled monolayers (SAMs) based on n-octylphosphonic acid (C8PA) and 1H,1H,2H,2H-perfluorooctanephosphonic acid (PFOPA) were investigated for application as an anode buffer layer in C_{60}-based organic photovoltaic (OPV) devices. We found that the degradation of the OPV efficiency with respect to air exposure was significantly reduced with the perfluorinated PFOPA compared to the aliphatic C8PA. We attribute the OPV degradation to moisture diffusion from the top aluminum electrode and the lowering of the anode work function as a result of hydrolysis of the SAM buffer layer.

© 2014 Elsevier B.V. All rights reserved.

1. Introduction

The performance of an organic photovoltaic (OPV) device can be significantly affected by the hole (or electron) injection interface formed between the anode (or cathode) and the photoactive organic semiconductor layer. In general, appropriate alignment of the electrode work function with the transport energy level of the organic semiconductor is required to produce ohmic contacts and good OPV parameters [1]. In a typical OPV device, slight work function variations due to the chemical or physical changes of the electrode surface can lead to significant changes in the device parameters. This suggests that changes in the anode or cathode interfacial properties can be examined by monitoring the OPV parameters over

time and at different conditions. For the anode, indium tin oxide (ITO) is widely used because of its high optical transparency and relatively high work function. To further improve hole injection, various methods have been used to increase the work function of ITO [1–3]. One such method is to use a self-assembled monolayer (SAM) as a buffer layer between ITO and the hole-transport layer (HTL). By attaching an electron withdrawing or donating moieties to ITO via SAMs, the effective work function of the ITO electrode can be increased or decreased, respectively [4–6]. Various monolayers have been found to be useful, including phosphonic acids [7–12], silanes [13], and carboxylates [14,15]. Phosphonic acid SAMs are commonly used due to their covalent bonding with hydroxyl-terminated ITO surface and good stability in ambient environments [16]. In particular, fluorinated phosphonic acid monolayers have been found to be useful in improving the hole-injection contact [2,7], and consequently, the efficiency of solar cells [4] and organic light-emitting diodes (OLEDs) [12]. Although many reports have examined the effect of SAMs on device efficiency, their effect on device lifetime has seldom been reported [17]; and it is unclear if the molecular

---

* Corresponding authors at: University of Rochester, Department of Chemical Engineering, Rochester, NY 14627, USA.

E-mail addresses: alexander.shestopalov@rochester.edu (A.A. Shesto-palov), ching.tang@rochester.edu (C.W. Tang).

[1] These authors contributed equally to this study with FA responsible for OPV fabrication and characterization and YL for SAM preparation and characterization.

structures of SAMs, which in principle can be easily designed to produce enhanced efficiency in OPV devices, would have any correlation with the device stability. The aim of this investigation is to understand the degradation mechanisms in OPV devices related to SAMs that have been often used as electrode buffers in enhancing OPV efficiency. Specifically, we investigated two phosphonic acid monolayers – aliphatic C8PA and fluorinated PFOPA – as standalone films and as an anode buffer in C_{60}-based OPVs.

2. Experimental

OPV devices were fabricated on pre-patterned ITO (90–100 nm) glass substrates (1.5 × 1.5 inches) with a surface resistance of 15 Ω/sq and an optical transparency of ~90%. The ITO substrates were cleaned as follows: rinsing with ultra-pure water, 10 min agitation in an ultrasonic water bath, rinsing with isopropanol (IPA), and 10 min agitation in ultrasonic IPA bath. Following a final IPA rinse, the substrates were dried with nitrogen and treated with oxygen plasma (5 min, 55 W and 2.6×10^{-1} mbar) before use. For SAM deposition, the substrates were reacted in 10 mM solution of the respective C8PA and PFOPA in IPA for 18 h. They were then rinsed with IPA and dried in nitrogen. All solvents and solutions used for SAM deposition were filtered through a 0.2 µm PTFE filter. OPV devices were fabricated by vapor deposition under a vacuum of 5.0×10^{-6} Torr. MoO_x was deposited at 0.3 Å/s. TAPC (1,1-Bis-(4-bis(4-methyl-phenyl)-amino-phenyl)-cyclohexane), NPB (N,N′-Di-[(1-naphthyl)-N,N′-diphenyl]-1,1′-biphenyl)-4,4′-diamine) C_{60}, and Bphen (bathophenanthroline) were deposited at a 3 Å/s. Aluminum was deposited by e-beam at 6.0 Å/s. Four identical OPV devices with an active area of 0.1 cm^2 were produced on a single substrate. For the vacuum-air exposure sequence experiments, the devices were exposed to either: (a) laboratory ambient environment where the humidity, which varied from 42% to 66% of relative humidity, was not specifically controlled or (b) vacuum environment where the devices were kept in a chamber dried with drierite desiccant and evacuated to a pressure of 10 mTorr.

The current density–voltage (JV) characteristics were recorded with a Keithley 2400 source meter in the dark and under irradiation at 100 mW/cm^2 generated using an Oriel xenon lamp solar simulator equipped with an AM 1.5 G filter. The intensity was calibrated with a silicon photodiode traceable to National Renewable Energy Laboratory. Contact angles were measured with a VCA Optima automatic contact angle goniometer. The XPS spectra were recorded on a Kratos Axis Ultra DLD spectrometer with mono-Al X-ray source.

3. Results and discussion

3.1. Stability of C8PA and PFOPA monolayers on ITO at ambient conditions

We examined the stability of C8PA and PFOPA monolayers on ITO under various exposure conditions using water contact angle goniometry and X-ray photoelectron spectroscopy (XPS). For the goniometric analysis, the monolayers were analyzed using static water contact angle measurements to examine the polar interactions with the surface. Substitution of γ-ω hydrogens with fluorines in the alkane chain of the monolayer increases the contact angle from 91.3° (C8PA) to 107.7° (PFOPA), due to the hydrophobicity of the terminal CF_3 group (Table 1). The freshly formed monolayers were also exposed to water to test how they degrade in the presence of moisture over time. After 48 h exposure to water, the static contact angle of C8PA decreased to 50.2° suggesting partial or complete monolayer hydrolysis; the change for the PFOPA monolayer was less pronounced (99.7°), suggesting that it has higher stability in water than the C8PA and that it is less susceptible to hydrolysis.

XPS measurements confirmed the formation of the C8PA monolayer on ITO. The survey spectrum of C8PA on ITO contains peaks at 191 and 285 eV, which were assigned to P 2s and C 1s electrons from C8PA. In the narrow C 1s scan, the peak at 285.00 eV corresponds to the aliphatic carbons from the alkane chain and from the C—P bond. The origin of the peak at 288.5 eV is believed to come from ITO, which is typically contaminated with some form of C (Fig. 1). The survey spectra peaks of PFOPA on ITO at 191, 285, and 686 eV were assigned to P 2s, C 1s, and F 1s electrons from PFOPA. The C 1s narrow scan peaks at 285, 286, 288, 291, and 293 eV are assigned to C—C, C—P, ITO contamination, CF_2, and CF_3, respectively, confirming the formation of the PFOPA monolayer (Fig. 1).

After forming the monolayers, both substrates were exposed to various conditions, such as air (48 h), water (2 & 48 h), heat (80 °C for 2 h), and UV light at 254 nm (2 h) to examine their degradation at different ambient conditions. The densities of the monolayers before and after the exposure were compared using the C/(C + In), P/(P + In), and F/(F + In) (for PFOPA only) elemental ratios calculated from the narrow XPS scans. Table 2 demonstrates that after exposing the substrates to air for 48 h, the monolayers remained intact and retained much of their density. UV exposure for 2 h did not lead to noticeable changes in PFOPA monolayer density, while causing partial degradation of C8PA SAM. The exposure to heat at 80 °C for 2 h leads to the ~30% density decrease of C8PA SAM, while the PFOPA SAM composition remained unchanged. The most noticeable degradation in both monolayers was observed after they were exposed to water for 2 and 48 h. C8PA SAM demonstrated ~75% decrease in density after a 2 h exposure, while the PFOPA SAM density was reduced by only ~50%. Surprisingly, no additional degradation in the density of both SAMs was observed after a 48 h

Table 1
Water contact angle measurements of C8PA and PFOPA monolayers on ITO.

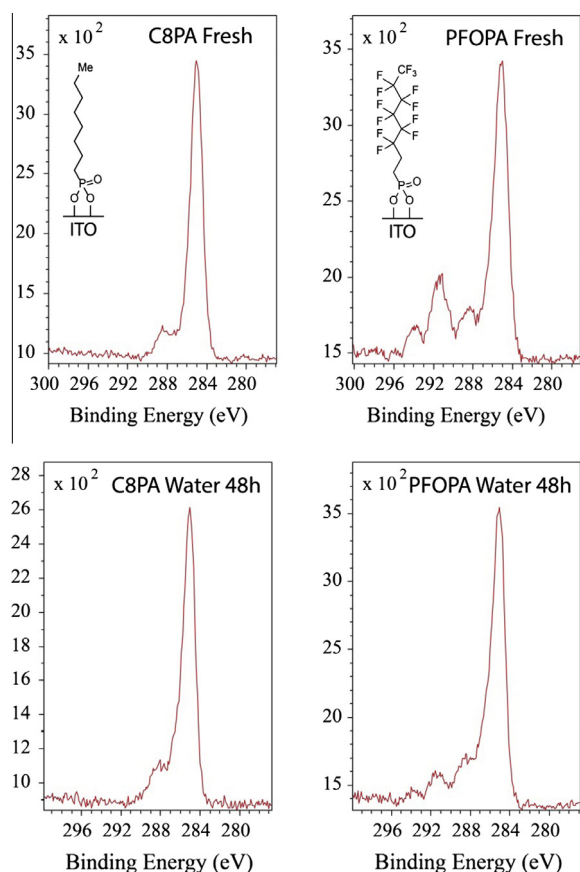| Exposure time (h)	C8PA		PFOPA	
	Air	Water	Air	Water
0	91.3		107.7	
1	96.0	51.2	108.0	99.7
24	97.4	51.5	110.0	100.7
48	97.8	50.2	83.0	99.7

Fig. 1. XPS spectra for C8PA and PFOPA monolayers.

Table 2
XPS analysis of C8PA and PFOPA monolayers on ITO.

P/(P + In)	C/(C + In)	P/(P + In)	C/(C + In)	F/(F + In)
C8PA SAM – Fresh		*PFOPA SAM – Fresh*		
1.53%	13.33%	1.29%	9.45%	10.58%
C8PA SAM – Air 48 h		*PFOPA SAM – Air 48 h*		
1.57%	13.84%	1.29%	9.78%	9.77%
C8PA SAM – UV 254 nm 2 h		*PFOPA SAM – UV 254 nm 2 h*		
1.32%	10.11%	1.30%	9.75%	11.31%
C8PA SAM – 80 °C 2 h		*PFOPA SAM – 80 °C 2 h*		
1.21%	9.81%	1.32%	9.03%	11.39%
C8PA SAM – Water 2 h		*PFOPA SAM – Water 2 h*		
0.40%	7.71%	0.66%	8.18%	4.78%
C8PA SAM – Water 48 h		*PFOPA SAM – Water 48 h*		
0.39%	7.62%	0.64%	8.14%	4.59%

exposure to water. Narrow carbon scans from both monolayers exposed to water retained all characteristic chemical states peaks (Fig. 1), suggesting only partial degradation of SAMs in water. These results suggest that (1) both monolayers are stable in air and that water causes their partial hydrolysis, and that (2) PFOPA SAM has higher tolerance towards hydrolysis in water and when heated, probably because of its higher hydrophobicity and decreased permeability towards polar molecules.

3.2. Stability of C8PA and PFOPA monolayers in OPV devices

The general OPV device structure for this study is: ITO/SAM/TAPC(5 nm)/C_{60}(40 nm)/Bphen(8 nm)/Al(100 nm). The TAPC layer is deliberately kept very thin to ensure that the open-circuit voltage (V_{oc}) is highly dependent on the SAM buffer. This structure is adapted from previous reports where MoO_x was used as the anode buffer [18,19]. Depending on the TAPC thickness, the V_{oc} achieved in ITO/MoO_x/TAPC/C_{60}/Bphen/Al devices can be significantly larger than what can be produced in a typical TAPC/C_{60} heterojunction device. Apparently, with a very thin TAPC layer (<10 nm) the built-in potential (V_{bi}) of TAPC/C_{60} heterojunction is not strictly determined by the HOMO–LUMO energy offset, but also influenced by the proximity of the heterojunction to the MoO_x buffer layer. The MoO_x buffer creates a Schottky-like anode contact with a barrier that affects the V_{bi} of the TAPC/C_{60} heterojunction. This MoO_x/TAPC/C_{60} device structure provides a simple method to probe the work function of the buffer anode layer based on the V_{oc} of the OPV device. Fig. 2 shows the initial JV characteristics obtained for a series of TAPC/C_{60} OPVs with: (1) ITO (control), (2) MoO_x, (3) C8PA, and (4) PFOPA as the buffered anode in contact with the TAPC layer and Bphen/Al as the buffered cathode. The V_{oc} correlates well with the work function of the SAM layer. PFOPA with a high work function of 5.3 eV produced a V_{oc} of 0.90 V compared to 0.50 V for C8PA with a low work function of 4.6 eV [7,12]. These literature work function values were obtained using a Kelvin probe in air. Although the absolute values of work function may be uncertain, they correlate well with V_{oc} of the OPV devices. Also expected is the higher V_{oc} (0.85 V) for MoO_x as compared to 0.60 V for the ITO control. All four devices showed similar values of short-circuit current density (J_{sc}) and fill factor (FF), except that the FF for MoO_x (0.55) is somewhat lower than the other devices (0.61–0.63).

In order to study the effect of SAMs on device stability, the OPV devices completed with the aluminum electrode were exposed to the following ambience sequence: vacuum for 48 h, air for 48 h, vacuum for 48 h and, finally, air for 24 h. The JV characteristics were recorded in air or vacuum, depending on the exposure. These experiments revealed that exposure of the OPV devices to air resulted in large efficiency degradation, whereas exposure to vacuum resulted in modest degradation. In both cases, the degradation is irreversible. Fig. 3 shows the evolution of V_{oc}, FF and J_{sc}, following this vacuum/air exposure sequence. Overall, the PFOPA device is much more stable compared to the C8PA device. Among the photovoltaic parameters, the J_{sc} is the most sensitive to air exposure while the V_{oc} the least. For the C8PA device, the J_{sc} decay is ~90% after 168 h compared to only 24% for the PFOPA device. Over the same period, the V_{oc} drop is only 30% and 11% for C8PA and PFOPA devices, respectively. For comparison, a V_{oc} drop of 42% for the control ITO device is the fastest whereas the V_{oc} drop for the MoO_x device is similar to the PFOPA device. The J_{sc} drop (~24%) for the MoO_x is also comparable to the PFOPA device, whereas the J_{sc} drop for the ITO device (50%) is between the two SAM devices.
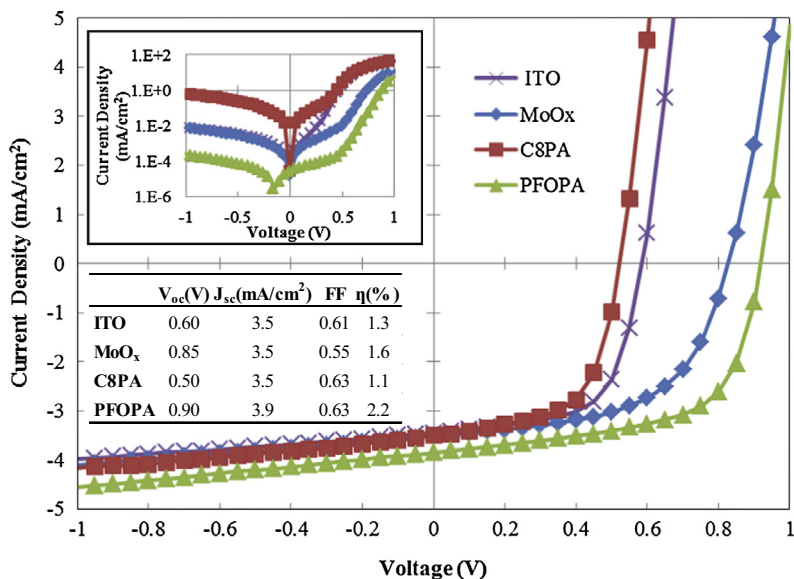
Fig. 2. Initial light JV characteristics for ITO, MoO$_x$, C8PA and PFOPA devices. Inset: dark J–V characteristics and data table.

The loss of J_{sc} can be attributed to a decrease in: (1) diffusion length of the photogenerated excitons, (2) exciton dissociation efficiency at the donor/acceptor interface, and (3) carrier collection at the electrodes. Previous reports have shown that exposure to oxygen and moisture has little effect on the absorption of C$_{60}$ films [20,21]. As shown in Fig. 4, the JV characteristics of PFOPA device after 168 h of air exposure maintain roughly the shape of the initial JV with only modest decrease in V_{oc} from 0.90 V to 0.80 V. In contrast, the C8PA device shows a substantial drop in V_{oc} from 0.50 V to 0.35 V in addition to a severe decrease in J_{sc}. The dark JV characteristics suggest that the contacts for both C8PA and PFOPA devices remain injecting despite degradation in work function. However, in the case of C8PA, a much lower V_{bi} may arise from a lower work function of the degraded C8PA buffered anode. As a result, the exciton dissociation at the TAPC/C$_{60}$ interface, and thus the $J_{sc,}$ is severely reduced. Along with the reduction in work function of the anode, another possible cause for the severe J_{sc} loss in the C8PA device is the accumulation of exciton quenchers at the TAPC/C$_{60}$ interface produced via chemical reactions involving C8PA. This degradation pathway has support in the behavior of the control ITO device, which showed even a larger decrease in V_{oc} but a smaller drop in J_{sc} compared to C8PA device. Fig. 5 shows the energy level diagrams for the OPV devices before (A) and after (B) 168 h of air exposure. In this diagram, the work function of the buffered anode is denoted ITO/φC8PA for the C8PA buffer and ITO/φPFOPA for the PFOPA buffer. The V_{bi} of the OPV device is controlled to a large degree by the buffer layer, which acts as a Schottky-like contact to the TAPC/C$_{60}$ heterojunction. V_{bi} is presumed to be proportional to the difference between the work function of the buffered anode and the C$_{60}$ LUMO. Upon atmosphere exposure, V_{bi} is decreased due to a reduction in the work function of this SAM buffered anode. This reduction apparently is much larger for C8PA compared to PFOPA, causing a larger decrease in both V_{oc} and J_{sc}.
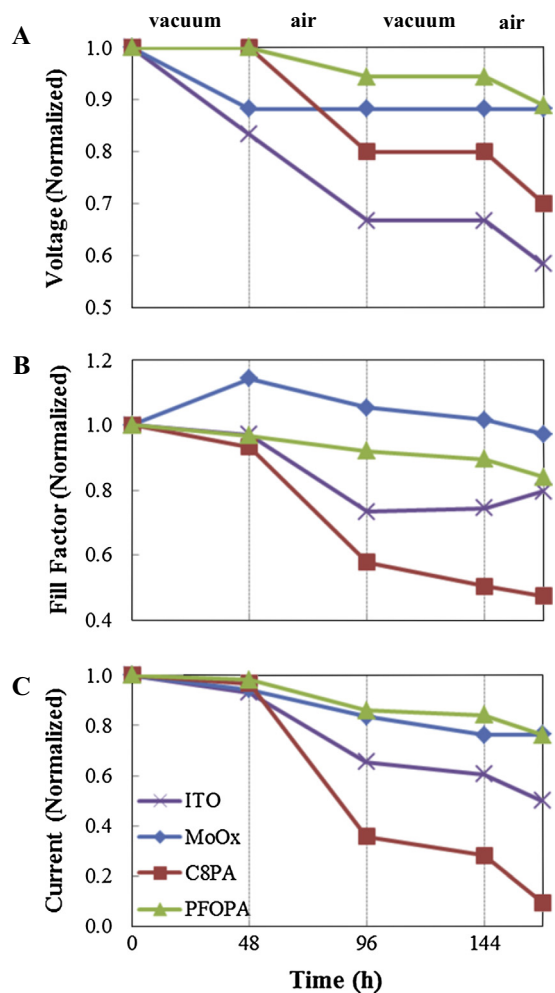

Fig. 3. Evolution of open circuit voltage (A), fill factor (B) and short-circuit current density (C) under vacuum/air exposure sequence.
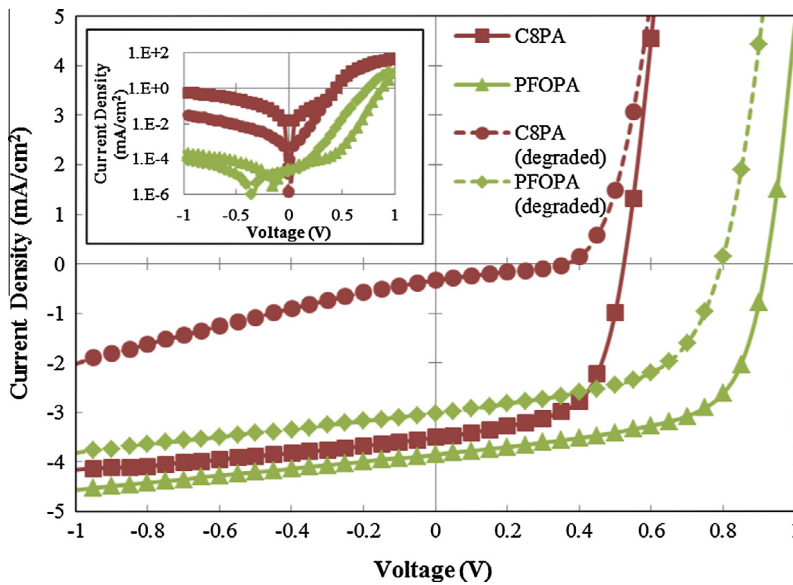
Fig. 4. Light JV characteristics for C8PA, PFOPA, degraded C8PA and degraded PFOPA devices. The degraded devices were exposed to air for 168 h. Inset: the corresponding dark JV characteristics.
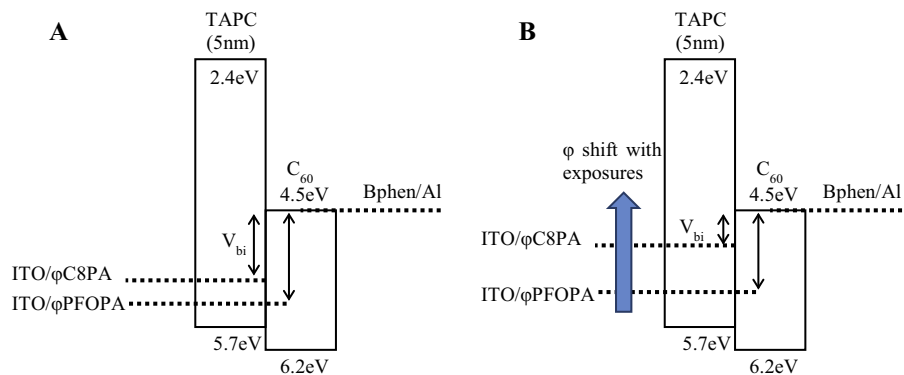

Fig. 5. Energy level diagrams for devices with SAMs as anode buffer layer before (A) and after (B) exposure to air for 168 h. The built-in potential (V_{bi}) is reduced by the upward work function (φ) shift of the ITO/SAM buffered anode with air exposure. The V_{bi} reduction is larger for C8PA compared to PFOPA.

To further understand the role of donor/C_{60} interface in the loss of J_{sc}, a set of devices with NPB as the donor was prepared for comparison with TAPC. NPB was selected because it is known to be more stable than TAPC in OLEDs under operational conditions [22]. In addition, NPB has a higher glass transition temperature (96 °C) than TAPC (79 °C) [23]. As shown in Fig. 6, the J_{sc} loss for the NPB devices with air exposure is comparable to the TAPC devices. Thus, it appears that the device degradation is more related to the instability of the SAM rather than the donor material.

OPV device degradation can be attributed to several factors including electro- and photo-chemical reactions involving the donor and acceptor molecules, and morphological and interfacial instabilities associated with the thin films. For OPVs with C8PA buffer as presented in this study, the device degradation could very well be dominated by the C8PA's propensity for hydrolysis. In our OPV devices, the source of moisture could come from adsorbed H_2O on
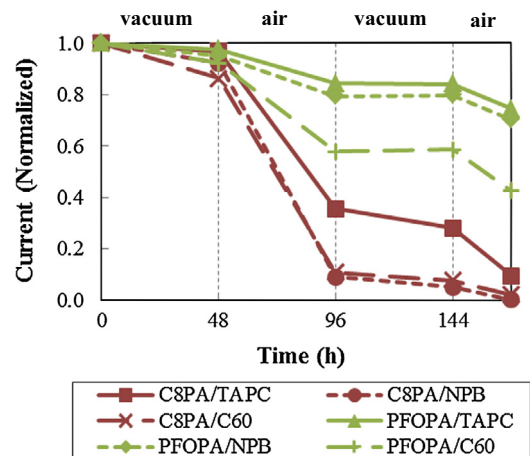

Fig. 6. Evolution of short-circuit current density for devices with various SAM/organic architectures under vacuum/air exposure sequence.

ITO surface from substrate preparation and SAM deposition. Moisture could also come from H_2O diffusion through the top aluminum electrode of the completed device upon air exposure [20,21].

In phosphonic acid monolayers, the phosphorous atom is bound to three oxygen atoms, which are capable of binding with a Lewis acidic metal [24]. Though there are different binding modes by which the phosphonic acid head group can bind to the surface of ITO (e.g. monodentate, bidentate, or tridentate modes), it has been suggested that the most common states of binding of C8PA to ITO are via bidentate and tridentate modes [25]. The P—O bonds are susceptible to water hydrolysis, which produces a free hydroxyl group on the phosphorous atom and decreases the degree of binding between the phosphonic acid and the ITO surface (Fig. 7). If sufficient hydrolysis occurs, it can lead to desorption of the entire molecule. Depending on the pH at the ITO/SAM interface, water hydrolysis can produce a positively-charged hydronium ion, which is also capable of diffusing back up through the SAM monolayer, going as far as the SAM/TAPC interface. Both the presence of a positively-charged species and the decrease in the binding mode can decrease the work function of ITO.

In order to evaluate the effect of moisture penetration, a set of devices was prepared with aluminum electrode of thickness from 100 nm to 200 nm. As shown in Fig. 8A, PFOPA devices are relatively unaffected by the electrode thickness. With a thicker electrode, the loss of J_{sc} in C8PA devices upon air exposure is significantly reduced. This suggests that moisture penetration through the aluminum electrode (via pinholes) is significant. In another experiment, a set of devices with TAPC thickness increased from 5 nm to 20 nm and aluminum electrode kept at 100 nm were subjected to vacuum/air exposure sequence. As shown in Fig. 8B, the effect on the J_{sc} loss is also significant for the C8PA devices. The effect on PFOPA devices is relatively minor regardless of the aluminum or TAPC thicknesses. These results suggest that moisture diffusion from aluminum electrode (exposed to air) could be the major source of degradation of OPV devices. As an anode buffer, C8PA, because of its lower hydrophobicity, is particularly sensitive to moisture induced degradation compared to PFOPA, which is more hydrophobic due to the fluorinated moieties. The much improved stability for the C8PA device with a thicker (20 nm) TAPC indicates that the TAPC/C_{60} heterojunction is relatively unaffected by the degradation in the C8PA modified ITO electrode. This suggests that the degradation species from hydrolysis of C8PA, if produced, are more localized at the ITO/C8PA interface and have little effect on the TAPC/C_{60} interface unless the TAPC layer is very thin.
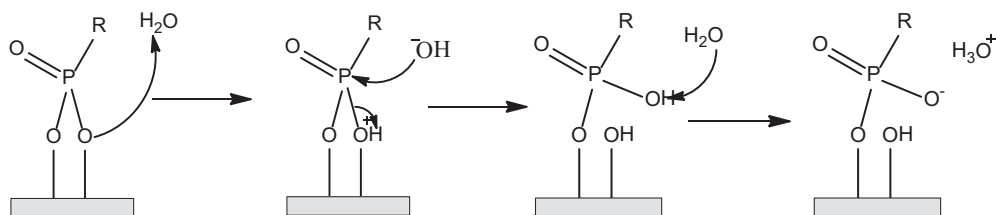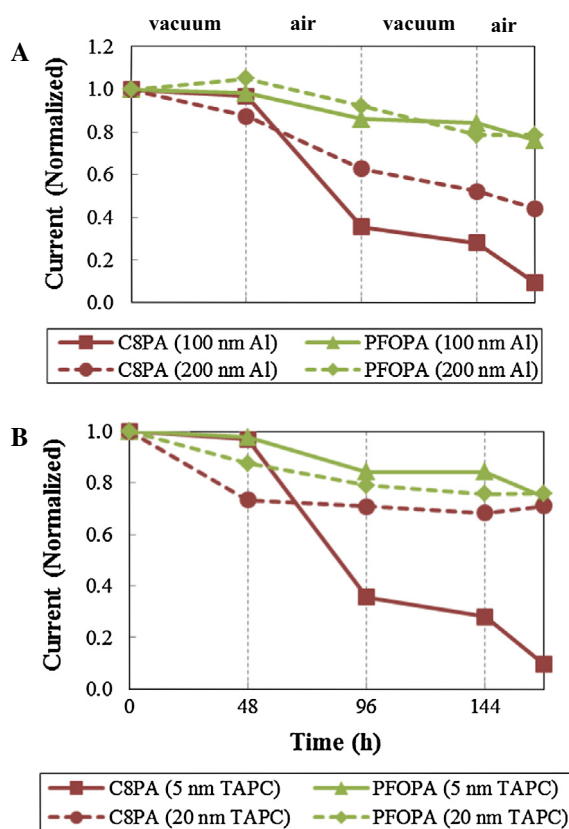

Fig. 8. Evolution of short-circuit current density for C8PA and PFOPA devices under vacuum/air exposure sequence. (A) Devices with 100 nm and 200 nm of aluminum; and (B) Devices with 5 nm and 20 nm of TAPC.

Water adsorption by C8PA and PFOPA monolayers could also be the source of moisture related to OPV device degradation. To assess this possibility, C8PA and PFOPA on ITO were first exposed to air for 48 h before completing the OPV devices with the remaining TAPC(5 nm)/C_{60}(40 nm)/Bphen(8 nm)/Al(100 nm) layers. Fig. 9 compares the initial JV characteristics of the devices with and without exposing C8PA and PFOPA to air. It can be seen that JV characteristics are only modestly affected by the exposure in both C8PA and PFOPA devices. This is in direct contrast with the severe degradation observed in the C8PA device (shown in Fig. 3) where the entire device is exposed to air. This suggests that OPV degradation is largely due to moisture penetration through the aluminum electrode and subsequent diffusion through the organic layer to cause reaction with SAM at the SAM/ITO interface. It is apparent that the amount of residue moisture at the ITO/SAM interface from
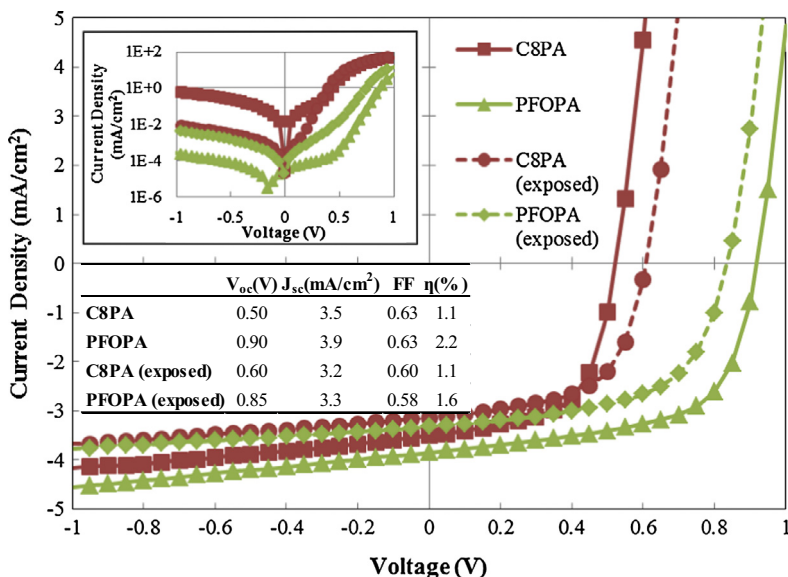

Fig. 7. Schematic representation of the hydrolysis of the P—O bond at the ITO surface.

Fig. 9. Initial light JV characteristics for C8PA and PFOPA devices. Exposed devices refer to fabrication with first exposing the buffer layers to air for 48 h before completing the device structure. Unexposed devices are those described in Fig. 2 shown here for comparison with exposed devices. Inset: corresponding dark JV characteristics and data table.

device fabrication, if present, is not significant. In addition, due to the device fabrication by vacuum deposition, any adsorbed moisture on the ITO/SAM substrate would be removed once the substrate is exposed to high vacuum (10^{-6} Torr) in the deposition coater over a typical process cycle. This suggests that the stability of a standalone SAM layer may have little correlation with the stability of the SAM/electrode interface in a working OPV device.

4. Conclusions

We investigated the degradation of C8PA and PFOPA self-assembled monolayers on ITO at ambient conditions and inside working OPV devices. Based on contact angle and XPS analysis, we showed that both C8PA and PFOPA SAMs are relatively stable and largely unaffected by prolonged air exposure. We also found that these two SAMs can affect the OPV device degradation very differently. As an anode buffer layer, C8PA caused rapid decrease in the short-circuit current with air exposure of the working device whereas the effect of PFOPA was relatively modest. We attribute the degradation to moisture diffusion from the top aluminum electrode and the lowering of the anode work function as a result of hydrolysis of the SAM layer at the ITO interface. Our results suggest that the apparent ambient stability of SAMs is not necessarily a good indicator of their utility as electrode buffers in OPV devices where the key device characteristics can be largely affected by minute changes in interfacial energetics.

Author contributions

All authors have contributed to the writing of the manuscript and given their approval to the final version.

References

[1] H. Ma, H.L. Yip, F. Huang, A.K.Y. Jen, Interface engineering for organic electronics, Adv. Funct. Mater. 20 (2010) 1371.
[2] R. Po, C. Carbonera, A. Bernardi, N. Camaioni, The role of buffer layers in polymer solar cells, Energy Environ. Sci. 4 (2011) 285.
[3] V. Shrotriya, G. Li, Y. Yao, C.-W. Chu, Y. Yang, Transition metal oxides as the buffer layer for polymer photovoltaic cells, Appl. Phys. Lett. 88 (2006) 073508.
[4] J.S. Kim, J.H. Park, J.H. Lee, J. Jo, D.-Y. Kim, K. Cho, Control of the electrode work function and active layer morphology via surface modification of indium tin oxide for high efficiency organic photovoltaics, Appl. Phys. Lett. 91 (2007) 112111.
[5] T. Xiong, D. Ma, The modification of self-assembled monolayer on indium tin oxide as cathode in inverted bottom-emitting organic light-emitting diodes, J. Appl. Phys. 104 (2008) 064506.
[6] C.M. Bowers, M. Zhang, Y. Lyubarskaya, E.J. Toone, C. Tang, A.A. Shestopalov, Structural modifications in bilayered molecular systems lead to predictable changes in their electronic properties, Adv. Mater. Interfaces 1 (2014) n/a.
[7] M. Wang, I.G. Hill, Fluorinated alkyl phosphonic acid SAMs replace PEDOT:PSS in polymer semiconductor devices, ACS Appl. Mater. Interfaces Appl. Phys. Lett. Org. Electron. 13 (2012) 498.
[8] M.D. Losego, J.T. Guske, A. Efremenko, J.-P. Maria, S. Franzen, Characterizing the molecular order of phosphonic acid self-assembled monolayers on indium tin oxide surfaces, Langmuir 27 (2011) 11883.
[9] T. Stubhan, M. Salinas, A. Ebel, F.C. Krebs, A. Hirsch, M. Halik, C.J. Brabec, Increasing the fill factor of inverted P3HT:PCBM solar cells through surface modification of Al-doped ZnO via phosphonic acid-anchored C60 SAMs, Adv. Energy Mater. 2 (2012) 532.
[10] J.A. Bardecker, H. Ma, T. Kim, F. Huang, M.S. Liu, Y.-J. Cheng, G. Ting, A.K.Y. Jen, Self-assembled electroactive phosphonic acids on ITO: maximizing hole-injection in polymer light-emitting diodes, Adv. Funct. Mater. 18 (2008) 3964.
[11] P.J. Hotchkiss, S.C. Jones, S.A. Paniagua, A. Sharma, B. Kippelen, N.R. Armstrong, S.R. Marder, The modification of indium tin oxide with phosphonic acids: mechanism of binding, tuning of surface

properties, and potential for use in organic electronic applications, Acc. Chem. Res. 45 (2012) 337.

[12] A. Sharma, B. Kippelen, P.J. Hotchkiss, S.R. Marder, Stabilization of the work function of indium tin oxide using organic surface modifiers in organic light-emitting diodes, Appl. Phys. Lett. 93 (2008) 163308.

[13] B. Choi, J. Rhee, H.H. Lee, Tailoring of self-assembled monolayer for polymer light-emitting diodes, Appl. Phys. Lett. 79 (2001) 2109.

[14] F. Nuesch, L. SiAhmed, B. Francois, L. Zuppiroli, Derivatized electrodes in the construction of organic light emitting diodes, Adv. Mater. 9 (1997) 222.

[15] D.H. Kim, C.M. Chung, J.W. Park, S.Y. Oh, Effects of ITO surface modification using self-assembly molecules on the characteristics of OLEDs, Ultramicroscopy 108 (2008) 1233.

[16] S.E. Koh, K.D. McDonald, D.H. Holt, C.S. Dulcey, J.A. Chaney, P.E. Pehrsson, Phenylphosphonic acid functionalization of indium tin oxide: Surface chemistry and work functions, Langmuir 22 (2006) 6249.

[17] H.B. Akkerman, A.J. Kronemeijer, J. Harkema, P.A. van Hal, E.C.P. Smits, D.M. de Leeuw, P.W.M. Blom, Stability of large-area molecular junctions, Org. Electron. 11 (2010) 146.

[18] M. Zhang, H. Wang, C.W. Tang, Effect of the highest occupied molecular orbital energy level offset on organic heterojunction photovoltaic cells, Appl. Phys. Lett. 97 (2010) 143503.

[19] M. Zhang, H. Wang, H. Tian, Y. Geng, C.W. Tang, Bulk heterojunction photovoltaic cells with low donor concentration, Adv. Mater. 23 (2011) 4960.

[20] K. Norrman, M.V. Madsen, S.A. Gevorgyan, F.C. Krebs, Degradation patterns in water and oxygen of an inverted polymer solar cell, J. Am. Chem. Soc. 132 (2010) 16883.

[21] M. Hermenau, M. Riede, K. Leo, S.A. Gevorgyan, F.C. Krebs, K. Norrman, Water and oxygen induced degradation of small molecule organic solar cells, Sol. Energy Mater. Sol. Cells 95 (2011) 1268.

[22] D.Y. Kondakov, Role of chemical reactions of arylamine hole transport materials in operational degradation of organic light-emitting diodes, J. Appl. Phys. 104 (2008) 084520.

[23] M. Aonuma, T. Oyamada, H. Sasabe, T. Miki, C. Adachi, Material design of hole transport materials capable of thick-film formation in organic light emitting diodes, Appl. Phys. Lett. 90 (2007).

[24] N. Sergent, P. Gelin, L. Perier-Camby, H. Praliaud, G. Thomas, FTIR study of low-temperature CO adsorption on high surface area tin(IV) oxide: probing Lewis and Bronsted acidity, Phys. Chem. Chem. Phys. 4 (2002) 4802.

[25] P.B. Paramonov, S.A. Paniagua, P.J. Hotchkiss, S.C. Jones, N.R. Armstrong, S.R. Marder, J.L. Bredas, Theoretical characterization of the indium tin oxide surface and of its binding sites for adsorption of phosphonic acid monolayers, Chem. Mater. 20 (2008) 5131.